NANO LETTERS

pubs.acs.org/NanoLett Letter

Unveiling the Interlayer Interaction in a 1H/1T TaS$_2$ van der Waals Heterostructure

Cosme G. Ayani,* Mihovil Bosnar,* Fabian Calleja, Andrés Pinar Solé, Oleksandr Stetsovych, Iván M. Ibarburu, Clara Rebanal, Manuela Garnica, Rodolfo Miranda, Mikhail M. Otrokov, Martin Ondráček, Pavel Jelínek, Andrés Arnau, and Amadeo L. Vázquez de Parga

Cite This: *Nano Lett.* 2024, 24, 10805−10812 **Read Online**

ACCESS | Metrics & More | Article Recommendations | SI Supporting Information

ABSTRACT: This study delves into the intriguing properties of the 1H/1T-TaS$_2$ van der Waals heterostructure, focusing on the transparency of the 1H layer to the charge density wave of the underlying 1T layer. Despite the sizable interlayer separation and metallic nature of the 1H layer, positive bias voltages result in a pronounced superposition of the 1T charge density wave structure on the 1H layer. The conventional explanation relying on tunneling effects proves insufficient. Through a comprehensive investigation combining low-temperature scanning tunneling microscopy, scanning tunneling spectroscopy, non-contact atomic force microscopy, and first-principles calculations, we propose an alternative interpretation. The transparency effect arises from a weak yet substantial electronic coupling between the 1H and 1T layers, challenging prior understanding of the system. Our results highlight the critical role played by interlayer electronic interactions in van der Waals heterostructures to determine the final ground states of the systems.

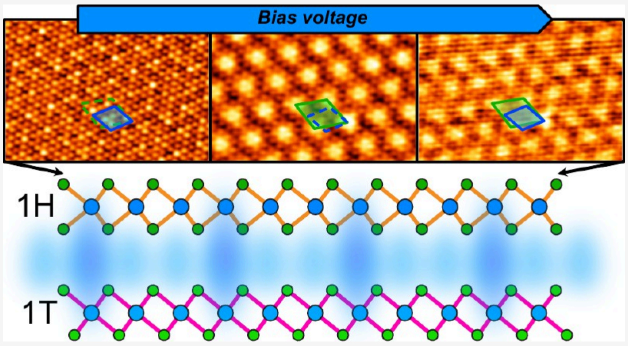

KEYWORDS: *Transition metal dichalcogenides, Tantalum disulfide, Van der Waals heterostructures, Density functional theory, Low temperature STM, Non-contact AFM*

In recent years, there has been a significant research focus on the exploration of two-dimensional (2D) materials. Following the groundbreaking isolation of graphene in 2004, interest has swiftly expanded to encompass a diverse array of 2D materials, including topological insulators, Xenes, perovskite-type oxides, and transition-metal dichalcogenides (TMDs), among others.[1]

The properties of these 2D materials can be finely tuned through various means, such as altering the number of layers, applying strain, adjusting the relative orientation between layers, or constructing van der Waals (vdW) heterostructures among others.[2,3] Transition-metal dichalcogenides, in particular, exhibit a multitude of intriguing phenomena, including Ising superconductivity, charge-density waves, metal−insulator transitions, and even a quantum spin liquid phase.[4−9] Their 2D nature enables the creation of vdW heterostructures by combining single layers of different TMDs, resulting in unique properties.[10,11] The emergence of novel properties in these heterostructures stems from weak interactions across the interfaces within the vdW assembly. Despite the wealth of studies published in recent years, the interlayer interactions in these vdW heterostructures remain poorly understood.

For example, consider the simplest heterostructure consisting of a bilayer formed by a layer of 1T-TaS$_2$ or 1T-TaSe$_2$, which exhibits a Mott insulating state associated with a Star-of-David (SoD) charge density wave (CDW),[4,5,12] and a layer of their 1H counterparts, that are metallic. Despite the coincidence in the experimental results measured by different groups, various theoretical proposals exist regarding the system's ground state. These proposals range from the formation of a Kondo lattice or a magnetically ordered state to the emergence of a spin liquid phase or its identification as a doped Mott system.[13−17]

As another example, we can consider the so-called "transparency effect" in 1H/1T-TaS$_2$ heterostructures. Low-temperature scanning tunneling microscopy (STM) images of the 1H layer at bias voltages in the range 100−250 mV clearly show the periodicity of the 1T CDW superposed onto the 1H surface.[18−23] The original explanation of this transparency effect assigns it to a purely tunneling effect, wherein electrons

Received: April 30, 2024
Revised: July 12, 2024
Accepted: July 15, 2024
Published: July 22, 2024

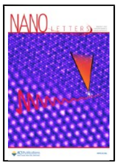

https://doi.org/10.1021/acs.nanolett.4c02068
Nano Lett. 2024, 24, 10805−10812

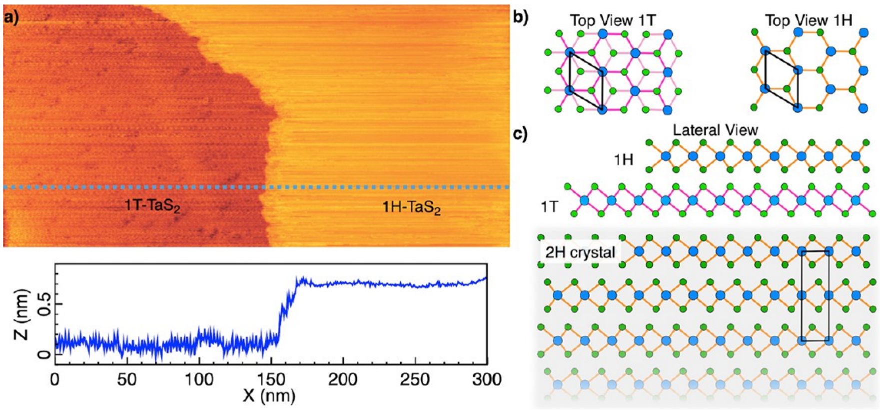

Figure 1. 1H/1T Heterostructure: (**a**) 300 nm wide STM image of the 1H/1T heterostructure and corresponding line profile below. The 1H and 1T surfaces are separated by a single layer step-edge of 680 ± 70 pm. Image parameters: $V_b = 300$ mV, $I = 100$ pA. (**b**) Ball models showing the top views of both the 1H and 1T phases; the blue balls represent the Tantalum atoms, the green balls represent the Sulfur atoms, and the orange and purple bonds represent the corresponding trigonal prismatic or octahedral coordination. (**c**) Lateral view of the 1H/1T heterostructure on the surface of the 2H-TaS$_2$ crystal; the vertical unit cell is marked with a black rectangle in the case of the 2H crystal, notice the 180° rotation every two layers.

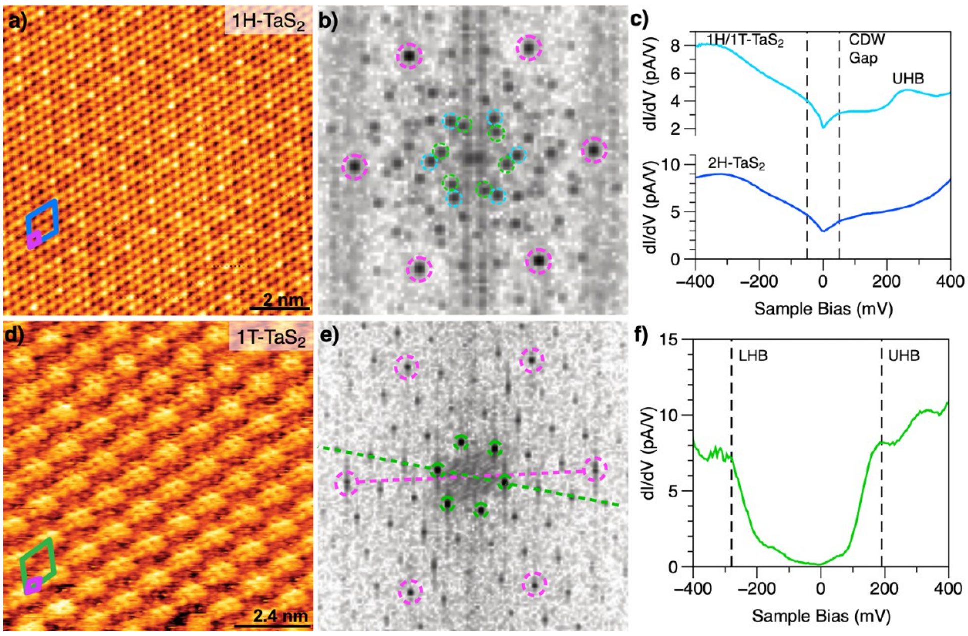

Figure 2. 1H/1T Heterostructure atomic and electronic properties: (**a**) STM topography image of the 1H surface where two periodicities are marked with two rhombi, in purple for the atomic lattice and blue for the quasi-(3 × 3) CDW (incommensurability discussion in section S2 of Supporting Information). Image parameters: $V_b = 100$ mV, $I = 300$ pA. (**b**) FFT of the STM image in panel (a), three periodicities are observed here and highlighted with circles. In purple the atomic lattice, in blue the quasi-(3 × 3) CDW, and in green the $(\sqrt{13} \times \sqrt{13})$R13.9° CDW of the 1T layer underneath. (**c**) STS point spectra of the 1H and 2H surfaces are shown in light blue and dark blue, respectively. The main difference in the LDOS of the 1H layer is the hump at 260 mV marked as UHB. STS parameters: $V_b = 400$ mV, $I = 500$ pA, $V_{mod} = 4$ mV. (**d**) STM atomically resolved topography image of the 1T surface, the periodicities are marked with two rhombi, purple for the atomic lattice and green for the $(\sqrt{13} \times \sqrt{13})$R13.9° CDW. Image parameters: $V_b = 100$ mV, $I = 300$ pA. (**e**) FFT of the 1T surface, the atomic and CDW periodicities are highlighted with purple and green circles, respectively. (**f**) STS point spectrum of the 1T surface where the positions of the upper Hubbard band (UHB) and lower Hubbard band (LHB) are marked. STS parameters: $V_b = 500$ mV, $I = 500$ pA, $V_{mod} = 5$ mV.

tunnel from the tip to the unoccupied states of a 1T layer through the 1H layer, assuming that the layers themselves are decoupled.[21−23] However, the tunneling current falls exponentially with distance, so given the large distance from tip to 1T layer due to the thickness of the 1H layer and the corresponding vdW gap, the signal coming from the 1T layer should be negligible in comparison to the 1H contribution. Furthermore, recent works have reported a subtle transparency effect even at negative bias voltages.[24,25] Therefore, a pure tunneling effect with decoupled 1H and 1T layers is an insufficient explanation, and there must be a different mechanism for such a clear transparency effect.

To unveil the origin of the coupling between layers, we investigated a vertical TaS$_2$ heterostructure featuring 1H and 1T monolayers naturally stacked on a 2H-TaS$_2$ crystal using low-temperature STM, scanning tunneling spectroscopy (STS), Kolibri non-contact atomic force microscopy (NC-AFM), and first-principles calculations. Our data analysis leads

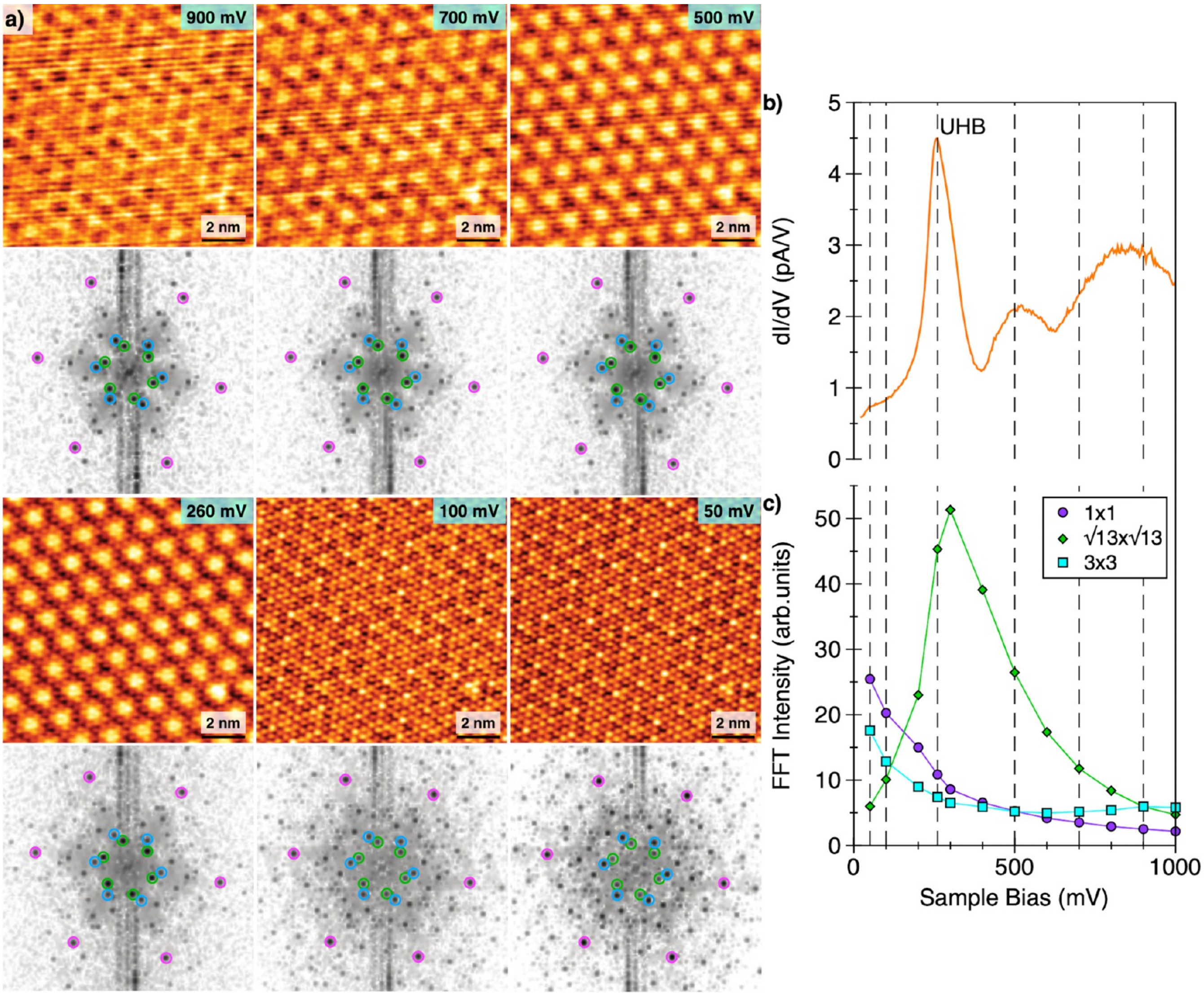

Figure 3. Transparency effect in STM: (**a**) STM Images and corresponding FFT plots performed on the 1H surface for different values of the bias voltage (V_b), the voltage value of the image is shown on the top right corner of the images. All STM images are scanned at a current of 300 pA. (**b**) dI/dV spectrum performed on the same 1H area with the same tip used to perform the bias voltage series images shown in panel (a). The bias voltage at which the images are taken is marked in the spectrum with black dashed lines; the hump observed at 500 mV is produced by the upper edge of the lowest 1H conduction band. The feature measured at +260 mV is related with the Upper Hubbard band from the 1T layer.[32] STS parameters: V_b = 1 V, I = 700 pA, V_{mod} = 4 mV. (**c**) Plot of the absolute intensity of the 1st-order FFT spots for each periodicity as a function of the sample bias voltage.

us to an alternative explanation of the origin of the 1H layer transparency effect, which accounts for the strength of the 1T signal: it is clearly produced by a weak hybridization between the 1H and the 1T layer underneath, and, thus, it involves interaction between the layers of the vdW heterostructure.[26] We believe that this electronic coupling between layers must be considered when explaining all phenomena concerning TaS_2 systems and also that this weak but substantial electronic interaction between layers should be considered to understand the phenomena appearing in analogous 2D vdW heterostructures.[13−17]

TaS_2 is a transition-metal dichalcogenide which has two basic structures: the 2H-TaS_2 structure where the coordination between the Ta and S atoms is trigonal prismatic, and the 1T-TaS_2 structure with an octahedral coordination;[18] both polymorphs are very close in energy[19,27] and therefore coexist like in the 4Hb-TaS_2 crystals. The 2H-TaS_2 undergoes an in-plane transition around 78 K with a long-range quasi-commensurate (3 × 3) CDW[28,29] while 1T-TaS_2 polymorph presents, below 180 K, a commensurate CDW with a periodicity of $(\sqrt{13} \times \sqrt{13})R13.9°$.[18,30] The 1H/1T van der Waals heterostructures are studied on a 2H-TaS_2 single crystal cleaved in ultrahigh vacuum (UHV) and transferred into the STM at 1.2 K without breaking the UHV conditions. As investigated with STM, the sample surface of the 2H-TaS_2 crystal presents wide and clean terraces separated by single layer steps. In some cases, as in the example depicted in Figure 1(a), the upper and the lower terrace present different periodicities and corrugations. The line profile shows an apparent step height of 680 ± 70 pm and a difference in corrugation between the lower and upper terrace. Figure 2(a,d) shows atomically resolved STM images acquired in the upper and lower terrace, respectively. The atomic periodicity is marked in both images with purple rhombi on both images. In

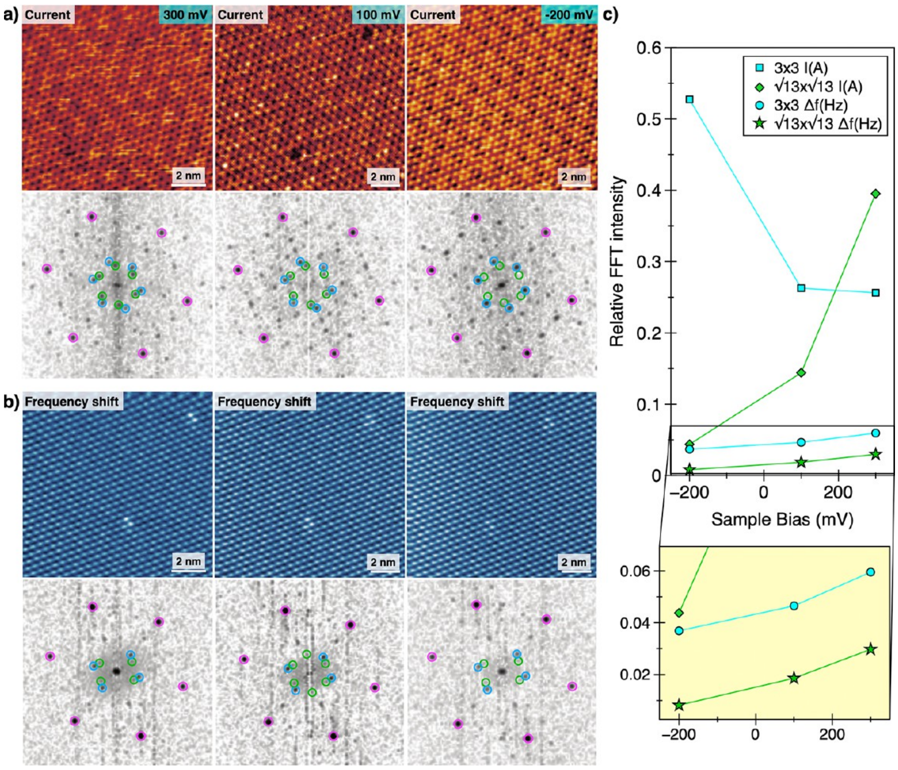

Figure 4. Transparency effect in AFM: (a) AFM images performed with a Kolibri sensor on the 1H surface. In this panel the current channel is depicted, and below each AFM image its corresponding FFT is shown where the 3 different periodicities are highlighted with circles. Only the voltage is varied between each image. **(b)** Same AFM image as the one shown in panel (a), but in this case the frequency shift channel is depicted; also, the corresponding FFT images are shown below. **(c)** The plot shows how the integrated intensity of the 1st-order FFT spots for each periodicity of the current and frequency shift channel changes as the bias voltage is ramped. In this case the FFT intensity is normalized with respect to the intensity of the atomic periodicity FFT spots. The zoom below shows a closer look at the frequency shift results. Image parameters: $I = 10$ pA, -1.15 Hz $< \Delta f <$ 0.058 Hz.

Figure 2(a) the quasi-(3×3), corresponding to the 1H CDW, is marked with a blue rhombus. In Figure 2(d), the $(\sqrt{13} \times \sqrt{13})R13.9°$ periodicity, corresponding the 1T CDW, is marked with a green rhombus (see all values in section S1 of the Supporting Information). Figure 1(b) shows the top view of the two polymorphic structures with the black rhombus indicating the surface atomic periodicity. Figure 1(c) shows the lateral view of the stacking sequence corresponding to the area shown in Figure 1(a), a naturally occurring 1H/1T bilayer heterostructure in the topmost layers of the 2H-TaS$_2$ crystal.

Figure 2(b,e) shows the fast Fourier Transform (FFT) of the images. In panel (e) the dots corresponding to the atomic periodicity are marked with a purple dashed circle, and the ones corresponding to the $(\sqrt{13} \times \sqrt{13})R13.9°$ periodicity are marked with green dashed circles. In panel (b) the atomic periodicity is marked with purple dashed circles, the blue dashed circles indicated the quasi-(3×3) periodicity, and finally, despite the fact that the image has been acquired on the 1H terrace, the periodicity of the $(\sqrt{13} \times \sqrt{13})R13.9°$ is observed (green dashed circles). As can be seen, the atomic lattices on both polymorphs are aligned (see S3 in the Supporting Information).

Figure 2(c) shows the comparison between the dI/dVs measured on the 1H area (light blue) and the 2H crystal (dark blue). In both spectra the quasi-(3×3) CDW pseudogap appears at the Fermi level.[25,29,31] However, in the 1H areas we find a new feature between 230−260 mV, which has not been reported on previous works on 4Hb-TaS$_2$ crystals[25] and, in the case of 1H layers embedded in 1T-TaS$_2$ crystal, it may be sightly distinguished in a spectrum at 4.2 K shown in the Supporting Information of ref 27, but no explanation is given regarding its origin. Figure 2(f) shows the dI/dV measured on the 1T layer showing the presence of the upper and lower Hubbard band features.[32,33]

The topography and FFT image of the 1H surface already reveal the presence of the CDW from the 1T layer underneath; in essence, the images scanned over the 1H surface are bias-dependent, and the 1T CDW always appears superposed with varying intensity. This behavior suggests the presence of intricate electronic interactions between the 1H and 1T layers that are not immediately evident from direct tunneling considerations, as was already argued. In order to unveil these interactions, we have studied the intensity of both CDW periodicities on the 1H surface for a wide range of positive bias voltages by means of FFT analysis of STM and AFM images in order to track their bias voltage dependence. All the results are depicted in Figure 3 and Figure 4.

Figure 3 shows the results regarding STM data; in panel (a), six STM images from a voltage series out of a total of 12 are depicted. The bias voltages at which the STM images are scanned are also marked on the STS spectrum of panel (b), which was acquired on the same area and with the same tip used to complete the whole bias voltage series. Two spectral features are identified in the STS spectrum; one is the upper edge of the 1H layer conduction band that is resolved at 500 mV, and the second is a prominent peak at +260 mV that roughly corresponds to the energy position of the UHB on the 1T phase underneath. The results of the bias voltage series are

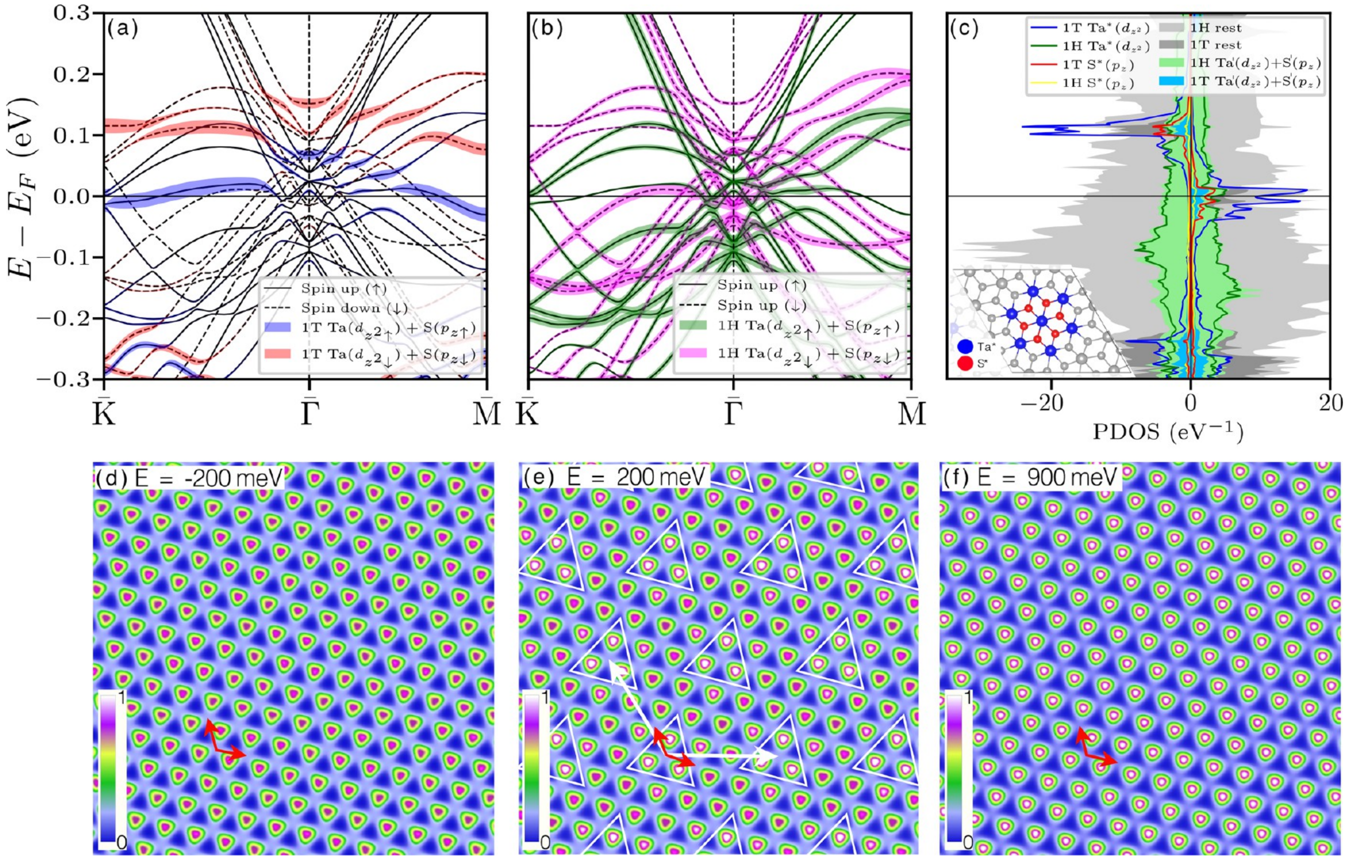

Figure 5. Explanation of the transparency effect: Electronic band structure of the 1H/1T bilayer with fat bands showing contributions of dominant out-of-plane orbitals Ta(d_{z^2}) and S(p_z) stemming from **(a)** 1T and **(b)** 1H layers. The PDOS analysis, panel **(c)**, shows that the nondispersive Hubbard bands are predominantly localized on the Ta atom at the center of the star-of-David distortion in the 1T layer and the closest Ta* and S* atoms (see the inset). The 1H Ta* and S* atoms are those closest to the 1T and S* atoms. The prime symbol [′] denotes all other Ta and S atoms in the heterostructure. Spin up and spin down channels appear in the right and left panels, respectively. The corresponding DOS contributions resonate with the contributions of the out-of-plane orbitals of atoms in the 1H layer above them, resulting in a noticeable hybridization. Panels **(d−f)** show simulations of constant height integrated LDOS above the 1H layer. In panel (d), the energy integration interval does not contain the band crossings due to 1H-1T hybridization, and the LDOS shows a (1 × 1) pattern (red arrows). In panel (e), this interval includes the band crossings, and the LDOS instead shows a ($\sqrt{13} \times \sqrt{13}$) pattern (white arrows denote the periodicity). The white triangles are centered on Ta atoms at the center of the star-of-David distortion and serve as guides to the eye. In panel (f), the energy range is increased further to 900 meV, and the ($\sqrt{13} \times \sqrt{13}$) pattern is muted due to the small hybridization contribution compared to the total DOS (cf. the contribution of the rest of the system in panel (c)). The inset in panel (c) was produced with the VESTA package,[34] while the LDOS plane cuts were produced by XCrySDen package.[35]

summarized in panel (c). Here, the intensity of the first-order FFT spots for the three different periodicities is plotted as a function of the bias voltage of the corresponding STM image. From both the STM images and the integrated FFT intensity plot, we can conclude that there is an inversion in the intensity of the CDWs at 100 mV below which the quasi-(3 × 3) dominates the topography of the 1H surface. For higher bias voltages the relation is the opposite; the superimposed ($\sqrt{13} \times \sqrt{13}$)R13.9° becomes more intense following the same trend described in previous works.[21−24]

However, some differences and new information can be extracted from the FFT intensity plot in Figure 3(c). Above 900 mV, the intensities of both superstructures are practically the same, the intensity of the quasi-(3 × 3) being slightly higher for 1 V. As the voltage is decreased, the intensity of the ($\sqrt{13} \times \sqrt{13}$)R13.9° CDW spots increases, reaching a maximum at 300 mV and then falling rapidly. Comparing panels (b) and (c) of Figure 3, we can see that the maximum intensity of the ($\sqrt{13} \times \sqrt{13}$)R13.9° reconstruction is reached precisely in the vicinity of the +260 mV UHB feature and then decreases for lower voltages. To further confirm the relation between the STS feature and the 1T CDW periodicity, we have performed STS point spectra following the periodic unit cell of the ($\sqrt{13} \times \sqrt{13}$)R13.9° CDW superposed on the 1H layer. The results, shown in Figure S4 of the Supporting Information, indicate that the intensity maxima that appear in the dI/dV map at +260 mV correspond exactly to the 1T CDW maxima. Therefore, the +260 mV feature is spatially modulated with the 1T CDW that appears to be superimposed on the 1H layer. This effect is independent of the tip−sample distance (see sections S6 and S7 for detailed discussion).

Figure 4(a) shows the corresponding experimental results performed with an AFM; we show both the current channel, panel (a), and the frequency shift channel, panel (b). The results are condensed in the corresponding relative FFT intensity plot of panel (c). In this case, due to the large signal from the atomic lattice, as compared to the STM experiments, the FFT intensity of both CDWs is normalized to the atomic lattice for clarity. Regarding the current channel, the behavior is analogous to the one observed in the STM, and even the crossover in intensities is also measured at 100 mV, acting as control measurements and ensuring that the results of the frequency shift channel are reliable. Surprisingly, in the frequency channel, we can resolve both CDWs as can be seen by the FFT analysis. However, unlike in the current channel, there is no crossover of intensities, and the quasi-(3 × 3) CDW dominates over the 1H surface. Also, comparing with both current and STM measurements the relative intensity of the CDW spots with respect to the atomic lattice is much lower, representing always less than 6% of the atomic lattice intensity (see inset of Figure 4(c)). These results point in the direction that the transparency effect is mainly an electronic effect.

In order to clarify the origin of this electronic effect, we have performed state of the art DFT+U calculations. We consider as a minimal model the bilayer 1H-TaS_2/1T-TaS_2 heterostructure, i.e., the topmost two layers of the 1H/1T/2H heterostructure. The system is constructed following the approximation used in previous works,[15,16,36] where the lattice parameter of the ideal 1H layer in $(\sqrt{13} \times \sqrt{13})$ supercell is extended 1% to match the CDW reconstructed 1T layer (see Methods section and Supporting Information for details).

The calculated electronic structure of the model 1H/1T bilayer is presented in Figure 5. By comparing the fat bands corresponding to the 1T Ta(d_{z^2}) and S(p_z) orbitals in the heterostructure (panel (a)) with the bands of freestanding 1T (see Supporting Information, Figure S7), the lower and upper Hubbard bands can be identified. The lower Hubbard band is partially occupied, forming two electronic pockets near the 2D Brillouin zone boundary points K and M, while the upper Hubbard band is found at 100 meV above the Fermi level. The fat bands corresponding to the same orbitals of 1H (panel (b)) show that the Hubbard bands also have a small amount of these 1H contributions, suggesting that hybridization is taking place. In fact, the projected density of states (PDOS), panel (c), shows that the largest 1H contributions to the 1T Hubbard bands come from the 1H atoms closest to the center of the star-of-David distortion.

This hybridization can be visually connected with the transparency effect using local density of states (LDOS) calculations. Figure 5(d−f) shows the plane cut of the LDOS directly above the outer S atoms of the 1H layer integrated in different energy intervals. In the interval from $E_F - 200$ meV to E_F most of the bands have 1H character, and therefore, the corresponding LDOS (panel (d)) above the 1H layer has its 1 × 1 periodicity. In the interval from E_F to $E_F + 200$ meV, where the hybridization of 1T Hubbard bands with 1H bands was found to occur, the LDOS acquires the $(\sqrt{13} \times \sqrt{13})$ periodicity instead (panel (e)). When the integration is extended to a larger interval, e.g., from E_F to $E_F + 900$ meV as in panel (f), the $(\sqrt{13} \times \sqrt{13})$ periodicity in LDOS is again not visible because there are many additional 1H bands that are not hybridized with the 1T Hubbard bands. This behavior of the LDOS agrees with the STM observation shown in Figure 3(a).

Note that, while the agreement of our model and the experimental results shows that this model can explain the origin of the transparency effect, one must be aware of its limitations. In particular, the energy position of the calculated Hubbard bands does not match the observed features in STS. For example, the UHB is observed at 260 mV in STS, while it appears at around 100 meV in our calculations. Nevertheless, what matters is that, regardless the energy position of the Hubbard bands, the 1H and 1T hybridization should happen if (i) atoms are close enough for S(p_z) orbitals in the 1H and 1T layers to have a sizable overlap and (ii) 1H bands resonate with the states of the 1T Hubbard bands, for which there is a relatively wide energy window as seen in Figure 3(a,b).

The use of low-temperature STM and noncontact AFM has enabled us to characterize the geometric and electronic structure of 1H/1T TaS_2 heterostructure on a 2H crystal, finding the transparency effect of the 1H layer and an additional intriguing feature that appears in the 1H LDOS around +260 mV. Our results show that there is a weak, although sizable, coupling between the 1H and 1T layers. It is weak enough to maintain the structural properties of the vertical 1H/1T heterostructure with the same atomic lateral spatial periodicity, as well as the two CDWs periodicities of the pristine 1H and 1T layers, respectively, the quasi-(3 × 3) and $(\sqrt{13} \times \sqrt{13})R13.9°$ periodicities. However, this coupling between the 1T and 1H layers is strong enough to introduce hybridization between 1T and 1H electronic bands. A robust proof of this coupling is the observation of the 1T $(\sqrt{13} \times \sqrt{13})R13.9°$ periodicity on the 1H layer in STM images, happening for certain values of the applied bias voltage that fall close to the position of the UHB hybridized with the 1H bands.

In combination with the results of first-principles DFT calculations for a model 1H/1T TaS_2 bilayer, we have succeeded in giving a physical explanation to this so-called transparency effect that is beyond a pure tunneling effect simply based on the uncoupled electronic densities of the 1T and 1H layers. Our electronic band structure and projected density of states analysis shows that hybridization between bands with 1T and 1H character near the Fermi level appears at relatively large van der Waals interlayer distances but close enough to have overlap between S(p_z) orbitals in the 1H and 1T layers. In particular, the hybridization of the nondispersive pristine upper Hubbard band in the 1T layer with $(\sqrt{13} \times \sqrt{13})R13.9°$ CDW with unoccupied bands near the Fermi level in the 1H layer translates into local density of states modulation in the 1H layer with this periodicity, as observed in the STM images.

This case study emphasizes the significance of interlayer interactions in a specific TaS_2 van der Waals heterostructure, with potential applicability to analogous systems where these weak interactions are a cornerstone to understanding the reported low-temperature ground states.

■ ASSOCIATED CONTENT

Supporting Information

The Supporting Information is available free of charge at https://pubs.acs.org/doi/10.1021/acs.nanolett.4c02068.

> Both Experimental and DFT methods are included. All the values of the 1H and 1T layer periodicities are presented. The incommensurability of the quasi-(3 × 3) CDW is demonstrated via FFT study of STM images. Similar technique is used to determine the rotation between the 1H and 1T layers. Defects of the 1T layers are studied via noncontact AFM. The spatial modulation of the UHB is viewed via d*I*/d*V* intensity map of spectra performed along a 17 nm lime on the 1H surface. The effect of tip−sample distance in the transparency effect is studied via two experiments. The 1H/1T structural model used in the calculations, additional insights into

the 1H/1T electronic structure within DFT, the transparency effect vs interlayer distance variation, as well as the role of the Hubbard U parameter are also given (PDF)

AUTHOR INFORMATION

Corresponding Authors

Cosme G. Ayani − *Departamento de Física de la Materia Condensada, Universidad Autónoma de Madrid - Cantoblanco Campus, 28049 Madrid, Spain; IMDEA Nanociencia, 28049 Cantoblanco, Madrid, Spain;* orcid.org/0000-0002-3053-8579; Email: cosme.gonzalez@imdea.org

Mihovil Bosnar − *Departamento de Polímeros y Materiales Avanzados: Física, Química y Tecnología, Facultad de Ciencias Químicas, Universidad del País Vasco UPV/EHU, 20018 Donostia-San Sebastián, Spain; Donostia International Physics Center (DIPC), 20018 Donostia-San Sebastián, Spain;* orcid.org/0000-0002-3234-0179; Email: mihovil.bosnar@gmail.com

Authors

Fabian Calleja − *IMDEA Nanociencia, 28049 Cantoblanco, Madrid, Spain;* orcid.org/0000-0001-6007-8641

Andrés Pinar Solé − *FZU - Institute of Physics of the Czech Academy of Sciences, 16200 Prague 6, Czech Republic*

Oleksandr Stetsovych − *FZU - Institute of Physics of the Czech Academy of Sciences, 16200 Prague 6, Czech Republic*

Iván M. Ibarburu − *Departamento de Física de la Materia Condensada, Universidad Autónoma de Madrid - Cantoblanco Campus, 28049 Madrid, Spain; IMDEA Nanociencia, 28049 Cantoblanco, Madrid, Spain*

Clara Rebanal − *Departamento de Física de la Materia Condensada, Universidad Autónoma de Madrid - Cantoblanco Campus, 28049 Madrid, Spain; IMDEA Nanociencia, 28049 Cantoblanco, Madrid, Spain*

Manuela Garnica − *IMDEA Nanociencia, 28049 Cantoblanco, Madrid, Spain; Instituto Nicolás Cabrera (INC), Universidad Autónoma de Madrid - Cantoblanco Campus, 28049 Madrid, Spain;* orcid.org/0000-0002-7861-9490

Rodolfo Miranda − *Departamento de Física de la Materia Condensada, Universidad Autónoma de Madrid - Cantoblanco Campus, 28049 Madrid, Spain; IMDEA Nanociencia, 28049 Cantoblanco, Madrid, Spain; Instituto Nicolás Cabrera (INC) and Condensed Matter Physics center (IFIMAC), Universidad Autónoma de Madrid - Cantoblanco Campus, 28049 Madrid, Spain*

Mikhail M. Otrokov − *Instituto de Nanociencia y Materiales de Aragón (INMA), CSIC-Universidad de Zaragoza, 50009 Zaragoza, Spain*

Martin Ondráček − *FZU - Institute of Physics of the Czech Academy of Sciences, 16200 Prague 6, Czech Republic;* orcid.org/0000-0002-8808-1487

Pavel Jelínek − *FZU - Institute of Physics of the Czech Academy of Sciences, 16200 Prague 6, Czech Republic;* orcid.org/0000-0002-5645-8542

Andrés Arnau − *Departamento de Polímeros y Materiales Avanzados: Física, Química y Tecnología, Facultad de Ciencias Químicas, Universidad del País Vasco UPV/EHU, 20018 Donostia-San Sebastián, Spain; Donostia International Physics Center (DIPC), 20018 Donostia-San Sebastián, Spain; Centro de Física de Materiales CSIC/UPV-EHU-Materials Physics Center, E-20018 San Sebastián, Spain*

Amadeo L. Vázquez de Parga − *Departamento de Física de la Materia Condensada, Universidad Autónoma de Madrid - Cantoblanco Campus, 28049 Madrid, Spain; IMDEA Nanociencia, 28049 Cantoblanco, Madrid, Spain; Instituto Nicolás Cabrera (INC) and Condensed Matter Physics center (IFIMAC), Universidad Autónoma de Madrid - Cantoblanco Campus, 28049 Madrid, Spain;* orcid.org/0000-0003-0551-1603

Complete contact information is available at: https://pubs.acs.org/10.1021/acs.nanolett.4c02068

Author Contributions

◨C.G. Ayani and M. Bosnar contributed equally to this paper.

Notes

The authors declare no competing financial interest.

ACKNOWLEDGMENTS

This work has been supported by the Spanish Ministry of Science and Innovation, Grant Nos. PID2021-123776NBC21 (CONPHASETM), PID2019-103910GB-I00, PID2022-138210NB-I00, and PID2021-128011NB-I00 from MICIN/AEI/10.13039/501100011033 "ERDF A way of making Europe", also through "Severo Ochoa" (Grant CEX2020-001039-S) and "María de Maeztu" (Grant CEX2018-000805-M) Programmes for Centres of Excellence in R&D, respectively. The grant CEX2023-001286-S funded by MICIU/AEI/10.13039/501100011033 is also acknowledged. Additionally, computational resources were provided by the e-INFRA CZ project (ID:90254), supported by the Ministry of Education, Youth and Sports of the Czech Republic. Financial support has also been received by the Comunidad de Madrid (Project S2018/NMT-4511, NMAT2D) and the Basque Government IT-1527-22, as well as MCIN with funding from European Union NextGenerationEU (PRTR-C17.I1) promoted by the Government of Aragon. Financial support through the (MAD2D-CM)-MRR MATERIALES AVANZADOS-IMDEA-NC and (MAD2D-CM) MRR MATERALES AVANZADOS-UAM is also acknowledged. M.G. has received financial support through the "Ramón y Cajal" Fellowship program (RYC2020-029317-I) and "Ayudas para Incentivar la Consolidación Investigadora" (CNS2022-135175). M.O. and P.J. acknowledge the financial support from GACR project 20-13692X.

REFERENCES

(1) Khan, K.; et al. Recent developments in emerging two-dimensional materials and their applications. *J. Mater. Chem. C* **2020**, *8* (2), 387−440.

(2) Geim, A. K.; Grigorieva, I. V.; et al. Van der Waals heterostructures. *Nature* **2013**, *499* (7459), 419−425.

(3) Novoselov, K. S.; et al. 2D materials and van der Waals heterostructures. *Science* **2016**, *353* (6298), No. aac9439.

(4) Wilson, J. A.; et al. 2D materials and van der Waals heterostructures. *Adv. Phys.* **1975**, *24* (2), 117−201.

(5) Fazekas, P.; et al. Electrical, structural and magnetic properties of pure and doped 1T-TaS2. *Philos. Mag. B* **1979**, *39* (3), 229−244.

(6) Sipos, B.; et al. From Mott state to superconductivity in-1T-TaS 2. *Nat. Mater.* **2008**, *7* (12), 960−965.

(7) Tsen, A. W.; et al. Structure and control of charge density waves in two-dimensional 1T-TaS2. *Proc. Natl. Acad. Sci. U.S.A.* **2015**, *112* (49), 15054−15059.

(8) Xi, X.; et al. Ising pairing in superconducting NbSe2 atomic layers. *Nat. Phys.* **2016**, *12* (2), 139−143.

(9) Law, K. T.; et al. 1T-TaS2 as a quantum spin liquid. *PNAS USA* **2017**, *114* (27), 6996−7000.

(10) Sierra, J. F.; et al. Van der Waals heterostructures for spintronics and opto-spintronics. *Nat. Nanotechnol.* **2021**, *16* (8), 856−868.

(11) Guo, X.; Lyu, W.; Chen, T.; Luo, Y.; Wu, C.; Yang, B.; Sun, Z.; Garcia de Abajo, F. J.; Yang, X.; Dai, Q.; et al. Polaritons in van der Waals Heterostructures. *Adv. Mater.* **2023**, *35* (17), No. 2201856.

(12) Lee, S. H.; et al. Origin of the Insulating Phase and First-Order Metal-Insulator Transition in 1T-TaS2. *Phys. Rev. Lett.* **2019**, *122* (10), No. 106404.

(13) Vaňo, V.; et al. Artificial heavy fermions in a van der Waals heterostructure. *Nature* **2021**, *599* (7886), 582−586.

(14) Ruan, W.; et al. Evidence for quantum spin liquid behaviour in single-layer 1T-TaSe2 from scanning tunnelling microscopy. *Nat. Phys.* **2021**, *17* (10), 1154−1161.

(15) Wan, W.; et al. Evidence for ground state coherence in a two-dimensional Kondo lattice. *Nat. Commun.* **2023**, *14* (1), 7005.

(16) Crippa, L.; et al. Heavy fermions vs doped Mott physics in heterogeneous Ta-dichalcogenide bilayers. *Nat. commun.* **2024**, *15* (1), 1357.

(17) Ayani, C. G.; et al. Probing phase transition to a coherent 2D Kondo lattice. *Small* **2024**, *20* (8), No. 2303275.

(18) Coleman, R. V.; et al. Scanning tunnelling microscopy of charge-density waves in transition metal chalcogenides. *Adv. Phys.* **1988**, *37* (6), 559−644.

(19) Giambattista, B.; et al. Corrrelation of scanning-tunneling-microscope image profiles and charge-density-wave amplitudes. *Phys. Rev. B* **1988**, *38* (5), 3545.

(20) Fujisawa, Y.; et al. Superposition of ($\sqrt{13}\times\sqrt{13}$) and (3 × 3) supermodulations in TaS2 probed by scanning tunneling microscopy. *JPCS* **2018**, *969*, 012053.

(21) Han, W.; et al. Bias-dependent STM images of charge-density waves on TaS2. *Phys. Rev. B* **1994**, *50* (19), 14746−14749.

(22) Kim, J. J.; et al. Atomic- and electronic-structure study on the layers of 4Hb-TaS2 prepared by a layer-by-layer etching technique. *Phys. Rev. B* **1995**, *52* (20), R14388−R14391.

(23) Ekvall, I.; et al. Atomic and electronic structures of the two different layers in 4Hb at 4.2 K. *Phys. Rev. B* **1997**, *55* (11), 6758−6761.

(24) Wen, C.; et al. Roles of the narrow electronic band near Fermi level in 1T-TaS2 related layered materials. *Phys. Rev. Lett.* **2021**, *126* (25), 256402−1.

(25) Shen, S.; et al. Coexistence of Quasi-two-dimensional Superconductivity and Tunable Kondo Lattice in a van der Waals Superconductor. *Chin. Phys. Lett.* **2022**, *39* (7), No. 077401.

(26) Shao, B.; et al. Engineering Interlayer Hybridization in Energy Space via Dipolar Overlayers. *Chin. Phys. Lett.* **2023**, *40* (8), No. 087303.

(27) Wang, Z.; et al. Surface-Limited Superconducting Phase Transition on 1 T-TaS2. *ACS Nano* **2018**, *12* (12), 12619−12628.

(28) Nayak, A. K.; et al. Evidence of topological boundary modes with topological nodal-point superconductivity. *Nat. Phys.* **2021**, *17* (12), 1413−1419.

(29) Hall, J.; et al. Environmental Control of Charge Density Wave Order in Monolayer 2H-TaS2. *ACS Nano* **2019**, *13* (9), 10210−10220.

(30) Lefcochilos-Fogelquist, H. M.; et al. Substrate-induced suppression of charge density wave phase in monolayer 1HTaS2 on Au(111). *Phys. Rev. B* **2019**, *99* (17), 1−6.

(31) Wang, C.; et al. Spectroscopy of dichalcogenides and trichalcogenides using scanning tunneling microscopy. *J. Vac. Sci. Technol. B* **1991**, *9* (2), 1048.

(32) Qiao, S.; et al. Mottness collapse in 1T-TaS2-xSex transition-metal dichalcogenide: An interplay between localized and itinerant orbitals. *Phys. Rev. X* **2017**, *7* (4), 041054−10.

(33) Kim, J.-J.; et al. Observation of Mott Localization Gap Using Low Temperature Scanning Tunneling Spectroscopy in Commensurate 1T−TaS2. *Phys. Rev. Lett.* **1994**, *73* (15), 2103−2106.

(34) Momma, K.; et al. ıt VESTA3 for three-dimensional visualization of crystal, volumetric and morphology data. *J. Appl. Crystallogr.* **2011**, *44* (6), 1272−1276.

(35) Kokalj, A. XCrySDen - a new program for displaying crystalline structures and electron densities. *J. Mol. Graph. Mod.* **1999**, *17* (3), 176−179.

(36) Kumar Nayak, A.; et al. First Order Quantum Phase Transition in the Hybrid Metal-Mott Insulator Transition Metal Dichalcogenide 4Hb-TaS2. *Proc. Natl. Acad. Sci. U.S.A.* **2023**, *120* (43), No. e2304274120.